# Comparing the Effects of GPS Error on Different Electrical Resistivity Tomography Arrays for Archeological Investigations

Lorenzo Ciani, *Senior Member, IEEE*, Marcantonio Catelani, *Member, IEEE*, Giulia Guidi, *Student Member, IEEE*, Gabriele Patrizi, *Student Member, IEEE*, Luca Cappuccini, Nicola Casagli, Mattia Ceccatelli, and Veronica Pazzi

***Abstract*— An optimal reconstruction of the soil for archeological purposes is mandatory. Dimensions and depth of buried anthropogenic remains must be identified accurately allowing an easier design of the excavation survey and minimizing the excavation costs. Electrical resistivity tomography (ERT) is a widely used geophysical technique to measure the resistivity of the ground at different depths, and then reconstruct the underground stratigraphy. Misplacement of the electrodes is a fundamental aspect of these measurements because it could lead to incorrect data analysis. Regardless this issue, recent literature misses to consider the influence of the global position system (GPS) error in the localization of the electrodes on the final subsoil electrical resistivity distribution. In this article, the results of a measurement survey on the Poggio Pepe tumulus (Italy) were analyzed and a Monte Carlo (MC) simulation was carried out to investigate the influence of the GPS accuracy. The MC approach has been applied to two different kinds of ERT arrays: pole–dipole and dipole–dipole. Firstly, the simulation considers the ideal in-line position of the electrodes affected by the GPS error, then the real coordinates of the electrodes are introduced, together with the GPS uncertainty. The simulations provide interesting findings on how the GPS error influences the two arrays and the use of the topography. Moreover, the proper deployment of the remote pole for the pole–dipole array is discussed.**

***Index Terms*— Geophysical measurements, geophysics, measurement errors, soil measurements, tomography.**

## I. Introduction

A WIDELY employed technique in geophysical measurement is electrical resistivity tomography (ERT). It is used for environmental investigations [1]–[8], hydrogeology [9]–[11], civil engineering [12], [13], waste investigations [14], [15], and archeology [16]–[19]. This latter is a very challenging application field because of the complex subsoil resistivity distribution (buried anthropogenic structures can be identified by high resistivity anomalies at shallow depth), the target dimensions of few meters, and sometimes the rough topography (e.g., tumuli and/or funeral mounds) [18]–[22].

Despite the wide diffusion of the ERT measurements, this method is affected by problems. Noise contamination and high signal to noise ratio affect the quality of data, influencing resolution and reliability [14], [23]–[25]. In archeological applications, the resolution, for the identification of the dimensions and the depth of the buried objects, depends on the electrode spatial distribution [3], [17], [19]. Therefore, it is important to avoid as much as possible errors induced by the electrode distribution [26].

Zhou and Dahlin [25] suggest that there are two types of errors on ERTs: measured voltage errors and electrode-spacing errors. The first type could be caused by ineffective contacts between electrodes and soil (i.e., when the soil is rocky, or composed by gravels, or it is very dry so that the coupling between soil and electrodes is not suitable and the contact resistance is too high), damages to the cables, low injection current (so that the read voltage reaches the accuracy of the Voltmeter of the instrument), and background noises (i.e., an electrical line).

The second type could be caused by a wrong positioning of the electrodes (i.e., the electrodes are not placed at the fixed theoretical distance so that the spacing between two adjacent electrodes is lower/higher than the theoretical one) and/or by ignoring the topography (i.e., the real $x$-, $y$-, $z$-coordinates of each electrode) in the inversion procedure [23], [24], [27]–[30]. Electrode wrong positioning occurs always for some type of array (pole–dipole and pole–pole) because of the finite length of the cables that does not allow to place remote electrodes at infinite theoretical distance. Moreover, it can occur for human errors, when electrodes are posed by means of a tape or a string, and when electrodes have to be moved to improve the coupling with the soil. These sources of uncertainty could be reduced during the acquisition campaign but cannot be totally avoided.

Zhou and Dahlin [28] demonstrate that, when the theoretical fixed distance among the electrodes is equal or lower than 2 m, an electrode wrong positioning up to 10% could happen (i.e., if the fixed distance is 2 m, it is possible that an electrode has

Manuscript received April 6, 2020; accepted August 21, 2020. Date of publication September 3, 2020; date of current version November 17, 2020. The Associate Editor coordinating the review process was Chao Wang. *(Corresponding author: Lorenzo Ciani.)*

Lorenzo Ciani, Marcantonio Catelani, Giulia Guidi, and Gabriele Patrizi are with the Department of Information Engineering, University of Florence, 50139 Florence, Italy (e-mail: lorenzo.ciani@unifi.it; marcantonio.catelani@unifi.it; giulia.guidi@unifi.it; gabriele.patrizi@unifi.it).

Luca Cappuccini is with the Department of History, Archaeology, Geography, Fine and Performing Arts, University of Florence, 50124 Florence, Italy (e-mail: luca.cappuccini@unifi.it).

Nicola Casagli, Mattia Ceccatelli, and Veronica Pazzi are with the Department of Earth Sciences, University of Firenze, 50121 Florence, Italy (e-mail: nicola.casagli@unifi.it; mattia.ceccatelli@unifi.it; veronica.pazzi@unifi.it).

Digital Object Identifier 10.1109/TIM.2020.3021513

to be moved, for the above-mentioned reasons, up to 20 cm away from the theoretical position). Oldenborger *et al.* [23] calculate the dependence of data on the location of electrodes. Uhlemann *et al.* [8], studying the electrode's movements along a landslide, show that the knowledge of the exact position of the electrodes can avoid misinterpretations of the resistivity anomalies.

Nowadays, technology helps to mitigate electrode wrong position error, since the real/actual electrode location (in terms of $x$-, $y$-, $z$-coordinates) can be measured by laser distance meters ([24]) or by global position system (GPS) instruments [4], [8], [31], [32]. Nevertheless, employing GPS measurements, a new kind of error is introduced that related to the acquisition technique itself. The accuracy of GPS data, in fact, can be expressed as the product of the pseudo range error factor (UERE: user equivalent range error) and the geometry factor (DOP: dilution of precision) [33], [34]. The latter depends on the geometry of visible satellites: higher the value is, worse the satellite distribution over the horizon. In practice, the lower possible DOP value is around 2 [34]. The UERE value is obtained mitigating the error sources by means of: appropriate models, dual frequency receivers, number of visible satellites higher than 4, and adequate receiver shapes. The above-mentioned error sources are the following:

1) satellites and receiver clocks drift (clock-related errors);
2) ionosphere, troposphere, Earth rotation, and multipaths (signal propagation errors);
3) selective availability, signal jamming and spoofing (intentional errors);
4) orbital planes shape and receiver structure (system errors);
5) power failures and communication breakdowns.

The GPS error is widely studied in topography and geodesy, while recent geophysical literature does not take it into account. Therefore, it is mandatory to estimate how much the GPS uncertainty influences the soil resistivity measure. Starting from preliminary data analysis proposed in [35] and [36], this work illustrates some of the results of an ongoing project campaign on a great tumulus in Tuscany (Italy). A statistical analysis of the acquired data using Monte Carlo (MC) simulation is presented [37]–[41]. The purpose of the research is to investigate the effects of the errors occurred in collecting the electrode coordinates in two different array architectures, and to estimate if this effect has a relationship with the depth of investigation. Therefore, a comparison of four different scenarios is presented in order to highlight advantages and disadvantages of the methods and to find which is the best one for different applications. Furthermore, the optimal positioning of the remote pole is very challenging. In this work, a simulation of the remote pole positions (along $x$- and $y$-coordinates) is presented to find out the effects of a mispositioning in the resistivity output.

The data acquired on the Poggio Pepe tumulus are used as example to validate the procedure. The proposed approach is adaptable to any kind of ERT investigation even if the interpretation of the MC results depends on the field of application. Despite this, the findings of this article could be extended to any archeological survey (e.g., funeral mounds, walls, streets, etc.), because the depth of investigation range is usually comparable (approximately from 0 to 15 m). The optimization of the acquisition parameters is one of the key factors to reconstruct a more reliable subsoil model and improve the identification of the anomalies. Consequently, the archeological excavation survey can be designed easily, the research funding can be managed more efficiently, and the excavation survey costs can be minimized.

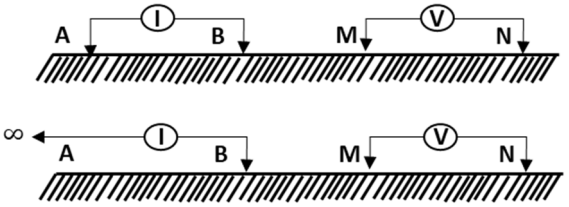


Fig. 1. Common arrays used in resistivity surveys. Top: Dipole–dipole configuration. Bottom: Pole–dipole configuration.

In Section II, the base theory of ERT measurement is explained; Section III describes the measurement survey carried out on the Poggio Pepe tumulus; Section IV proposes a MC-based approach to estimate the effects of the GPS error that affects the electrode coordinates measurement; and finally, Section V summarizes the main results and findings comparing four different models.

1) Pole–dipole array considering the theoretical in-line positions of the electrodes (fixed interspace).
2) Pole–dipole array considering the real 3-D topography (X; Y; Z coordinates).
3) Dipole–dipole array considering the theoretical in-line positions of the electrodes (fixed interspace).
4) Dipole–dipole array considering the real 3-D topography (X; Y; Z coordinates).

## II. ERT Measurement

The objective of ERT measurements is to determine the subsurface resistivity of the soil by means of measurements on the ground surface. The obtained resistivity value is not the true resistivity of the subsurface, but it is an "apparent" value that is the resistivity of a homogeneous ground that will give the same resistance value for the same electrode arrangement. The relationship between the "apparent" resistivity and the "true" resistivity is a complex relationship. Starting from the acquisition of the apparent resistivity it is possible to estimate the true resistivity of the subsurface ("inversion problem") [3], [16], [26], [42], [43]. There are several different array geometries used in ERT measurement (e.g. Wenner, Schlumberger, pole–dipole, dipole–dipole) [44]. Fig. 1 shows the deployment of the electrodes (commonly stainless-steel stakes insert in the soil for at least 1/3 of their length) in the considered geometry: dipole–dipole (D–D) on the top side and pole–dipole (P–D) on the bottom side. Both architectures are based on four electrodes, A and B are called current electrodes and $M$ and $N$ are called voltage electrodes. Using a set of batteries, a dc voltage is generated between the A and B electrodes, and

then the current I that flows between them is measured. At the same time, the voltage $\Delta V$ generated in the ground by the above-mentioned current is measured through two different electrodes ($M$ and $N$).

The current that flows through A and B generates a potential characterized by a symmetrical pattern about the vertical place at the midpoint between the two electrodes. The potential values in the M-electrode and N-electrode are given by equations (1) and (2) respectively,

$$\mathrm{V(M)} = \frac{\rho I_{\mathrm{AB}}}{2\pi}\left(\frac{1}{\mathrm{A\bar{M}}} - \frac{1}{\mathrm{B\bar{M}}}\right) \tag{1}$$

$$\mathrm{V(N)} = \frac{\rho I_{\mathrm{AB}}}{2\pi}\left(\frac{1}{\bar{AN}} - \frac{1}{\bar{BN}}\right) \tag{2}$$

where $\rho$ is the resistivity of the subsurface soil ("apparent") and $I_{\mathrm{AB}}$ is the current measured between A and B. Consequently, the measured voltage $\Delta V_{\mathrm{MN}}$ is given by

$$\Delta V_{\mathrm{MN}} = \frac{\rho I}{2\pi}\left(\frac{1}{\mathrm{A\bar{M}}} - \frac{1}{\mathrm{B\bar{M}}} - \frac{1}{\bar{AN}} + \frac{1}{\bar{BN}}\right). \tag{3}$$

The apparent resistivity $\rho$ is calculated using the measured current $I_{\mathrm{AB}}$ and the measured voltage $\Delta V_{\mathrm{MN}}$ as follows [45]:

$$\rho = k\frac{\Delta V}{I} \tag{4}$$

where $k$ is the geometric factor that depends on the arrangement of the four electrodes as follows:

$$k = \frac{2\pi}{\left(\frac{1}{\mathrm{A\bar{M}}} - \frac{1}{\mathrm{B\bar{M}}} - \frac{1}{\bar{AN}} + \frac{1}{\bar{BN}}\right)}. \tag{5}$$

The most commonly used arrays are (see Fig. 1) [3], [17], [18], [21], [22] as follows.

1) The dipole–dipole array is based on four aligned electrodes deployed using the sequence: *A, B, M,* and *N*. The lateral resolutions at shallow depths are enhanced using this configuration, as well as the electromagnetic inductive noise is minimized.
2) The pole–dipole array is based on three aligned electrodes (*B, M,* and *N*), and one current electrode (A) posed at theoretical infinite distance. This approach is characterized by high resolution and large depth of investigation.

Both P–D and D–D are characterized by two fundamental geometric parameters used to describe the sequence of acquisition during the measurement survey (see Fig. 2). The first one is the dipole length "a" defined as the distance between the two voltage electrodes in both array configurations, expressed in meters. In case of dipole–dipole, this factor must be also equal to the distance between the current electrodes. The second factor is the dipole separation factor "n," which is an integer value that indicates how many "a" there are between the current electrode B and the voltage electrode M.

In case of D–D array, introducing these two geometric parameters inside (5), the geometric factor $k_{\mathrm{DD}}$ could be revised as

$$k_{\mathrm{DD}} = \pi \cdot n \cdot (n+1) \cdot (n+2) \cdot a. \tag{6}$$

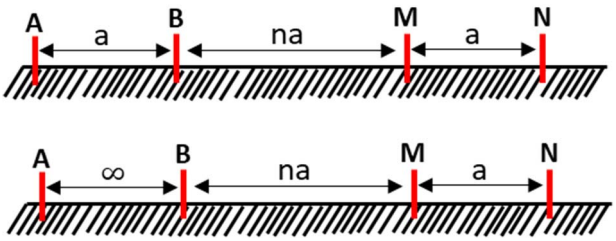


Fig. 2. Geometric parameters for dipole–dipole array (top) and for pole–dipole array (bottom). Red lines: electrodes. Shades: subsoil.

While, in case of P–D, the geometric factor $k_{\mathrm{PD}}$ could be revised as

$$k_{\mathrm{PD}} = 2\pi \cdot n \cdot (n+1) \cdot a. \tag{7}$$

ERT surveys are usually carried out using several electrodes directly connected to a resistivity meter system. This kind of instrumentation system is based on a microprocessor and an electronic switch to automatically select the relevant four electrodes for each acquisition. The microprocessor of the instrument needs to be programmed with sequence of measurements to take, the type of array used, and other survey parameters, e.g., the input voltage used to generate the current through the electrodes *A* and *B*. Using all this information the instrument automatically selects the appropriate set of electrodes for each measurement.

In case of dipole–dipole, the first step is to make all the possible measurements when the dipole length is "$a$ =1."

For the first measurement, the electrodes used are the numbers 1, 2, 3, and 4, while the second measurement is acquired using the electrodes 1, 2, 4, and 5. This is done up to the maximum dipole separation factor "n." After completing this sequence of measurement, the dipole length is increased to "a=2" and the process is repeated (the first with the electrodes 1, 3, 5, and 7). Then the dipole length "a" is increased up to its maximum value. The maximum of the parameters "n" and "a" are assessed depending on the maximum depth of investigation. In case of pole–dipole array the sequence of acquisition is still the same of the dipole–dipole one, but the electrode A is always placed at an infinite position.

According to [46], Table I illustrates the rule for the assessment of the depth of investigation $z_e$ based on the dipole separation and dipole length. Each acquisition included in the sequence is characterized by a determined value of the dipole separation "n" and the dipole length "a."

Selecting the proper row of Table I depending on "n" it is possible to obtain the corresponding $z_e/a$ value and consequently calculate the depth of investigation by multiplying this value for the corresponding "a." It is clear from the table that increasing "n" and/or "a" the depth of investigation increases.

## III. Measurement Survey

Vetulonia (Tuscany, central Italy) was one of the most important Etruscan towns. Many monumental tumuli were erected near it, one of them is the Poggio Pepe tumulus, one of the largest tumuli in Tuscany. This tumulus does not show any

morphologic deformation, suggesting that the internal structure of the tomb could be still intact.

An ERT survey was carried out on Poggio Pepe tumulus, with the aim to verify the presence of a tomb and optimize the archeological excavation. Seventy-two electrodes were placed in a linear configuration, with a theoretical electrodes space of 1.5 m, and a total linear length of 106.5 m. Furthermore, an extra-electrode called remote pole was installed as far as possible (at a theoretical infinite position) from the others at approximately 100 m perpendicularly far from the center of the linear array and it was used as A-electrode in the pole–dipole sequence of acquisition.

The data acquisition was carried out using a 10-channel receiver SyscalPro by Iris, equipped with 48 electrodes. Moreover, an external link (to reach a total amount of in-line 72 electrodes) was employed. The receiver was programmed to consider only 4 electrodes for each measurement, according to the procedure explained in section II. The instrument generates the data acquisition sequences considering 10 and 5 increments of "n" and "a," respectively. The number of possible combinations for the D–D array $C_{\mathrm{DD}}$ considering the procedure illustrated above is

$$C_{\mathrm{DD}} = \sum_{i=1}^{\alpha_{\max}} \sum_{j=1}^{n_{\max}} [N_{\mathrm{elect}} - (2\alpha_i + \alpha_i n_j)] \tag{8}$$

where $N_{\mathrm{elect}} = 72$ is the number of electrode used for this survey, $\alpha_i$ represents the increments of the dipole length "a," $n_i$ represents the increase of the dipole separation "n," $\alpha_{\max}$ and $n_{\max}$ are given by the following:

$$\alpha_{\max} = \left\lfloor \frac{N_{\mathrm{elect}} - 1}{3} \right\rfloor \tag{9}$$

$$n_{\max} = N_{\mathrm{elect}} - 1 - 2\alpha_i \quad \forall\, i = 1, 2, \ldots \alpha_{\max}. \tag{10}$$

While, the number of possible combinations for P–D array $C_{\mathrm{PD}}$ is

$$C_{\mathrm{PD}} = \sum_{i=1}^{\alpha_{\max}} \sum_{j=1}^{n_{\max}} [N_{\mathrm{elect}} - (\alpha_i + \alpha_i n_j)] \tag{11}$$

$$\alpha_{\max} = \left\lfloor \frac{N_{\mathrm{elect}} - 1}{2} \right\rfloor \tag{12}$$

$$n_{\max} = N_{\mathrm{elect}} - 1 - \alpha_i \quad \forall i = 1, 2, \ldots \alpha_{\max}. \tag{13}$$

Practically, to have a good signal to noise ratio, the increments of "a" are at least 5, while the one of "n" are between 6 and 10. In the presented study, the values of $\alpha_{\max}$ and $n_{\max}$ are fixed according to the geophysics literature equal to $\alpha_{\max} = 5$ and $n_{\max} = 10$, leading to $\alpha \in [1-5]$ and $n \in [1-10]$. In this scenario, the number of acquisitions for each ERT is given by

$$C_{\mathrm{DD}} = \sum_{i=1}^{5} \sum_{j=1}^{10} [72 - (2\alpha_i + \alpha_i n_j)] = 2475 \tag{14}$$

$$C_{\mathrm{PD}} = \sum_{i=1}^{5} \sum_{j=1}^{10} [72 - (\alpha_i + \alpha_i n_j)] = 2625. \tag{15}$$

In compliance with Table I, considering the maximum value of "n" and "a," the maximum investigation depths reached by D–D and P–D are 20 and 30 m, respectively.

TABLE I

PARAMETERS FOR THE IDENTIFICATION OF THE DEPTH OF INVESTIGATION ($z_e$) FOR THE DIFFERENT CONSIDERED ARRAY (DIPOLE–DIPOLE AND POLE–DIPOLE)

| Dipole separation | $z_e/a$ | |
|---|---|---|
| | Dipole-Dipole | Pole-Dipole |
| n=1 | 0.416 | 0.519 |
| n=2 | 0.697 | 0.925 |
| n=3 | 0.962 | 1.318 |
| n=4 | 1.220 | 1.706 |
| n=5 | 1.476 | 2.093 |
| n=6 | 1.730 | 2.478 |
| n=7 | 1.983 | 2.863 |
| n=8 | 2.236 | 3.247 |
| n=9 | 2.473 | 3.621 |
| n=10 | 2.712 | 3.996 |

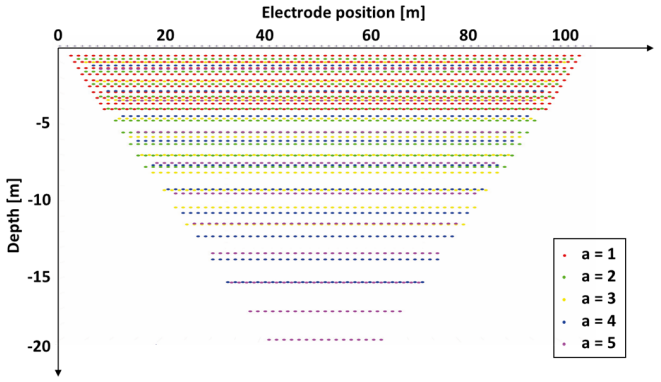


Fig. 3. ERT measurement diffusion underground. The sequence of acquisition was obtained for the dipole–dipole array with 72 electrodes, $a \in [1-5]$, and $n \in [1-10]$. Each color stands for a different value of "a," while the different section depths are obtained increasing "n".

Fig. 3 shows the results of the obtained sequence for the dipole–dipole array in the described scenario, in which each color represents a different value of the parameter "a," and each line of dots of the same color represents a different value of "n," where the higher the value of "n," the deeper the point of investigation.

Each dot in the figure stands for a point of investigation of the soil resistivity, placed in correspondence of the half distance between $A$ and $N$. The little black crosses just above the $x$-axis are the positions of the 72 electrodes. The figure highlights that the maximum depth of approximately 20 m could be obtained only with the maximum values of "a" and "n." Moreover, it reveals that there are many points of acquisition at shallow depth, while increasing the depth the number of points decrease since there are less acquisition with great values of "n."

The chosen instrument could work in two different modes of operation:

1) set a constant input voltage VAB selectable between the range from 12 to 800 V;

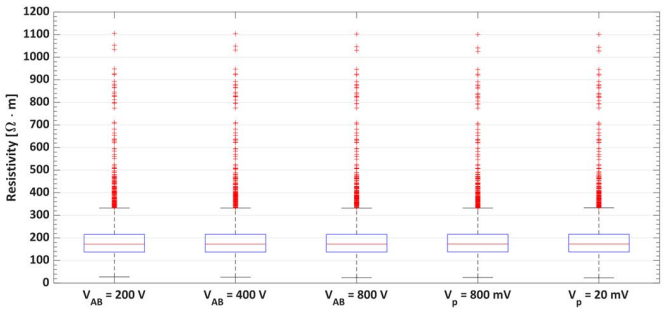


Fig. 4. Boxplots of dipole–dipole array resistivity acquired with different input voltages.

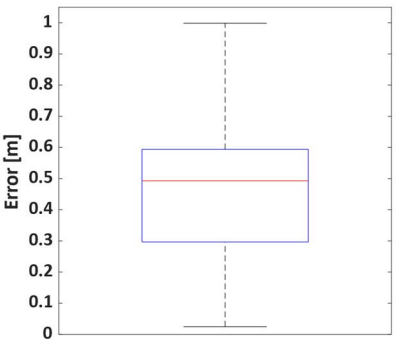


Fig. 5. Boxplot of all the errors in the GPS acquisition of the electrode position.

2) set a constant VP value, that has to be measured between $M$ and $N$ electrodes, between the range from 20 to 800 mV. The instrument varies the input voltage VAB that could be at least equal to a maximum value forced by the operator. The Save Energy Mode sets the voltage VP equal to 20 mV.

The survey was carried out using five input voltages for the dipole–dipole array ($V_{AB} = 200$ V; $V_{AB} = 400$ V; $V_{AB} = 800$ V; $V_P = 800$ mV; $V_P = 20$ mV), and two input voltages for the pole–dipole array ($V_{AB} = 800$ V; $V_P = 20$ mV). In both arrays, the maximum input voltage in the save energy mode was set to 800 V. Generally, the higher the voltage input, the better the quality of the data. On the other way, the use of low voltage allows to save batteries energy and repeat the measurement with different array displacements in the same day. However, these considerations are also strictly related to the type of soil investigated. For this reason, the survey was carried out using multiple input voltages. The results of the measurement campaign are summarized in Fig. 4, where each boxplot represents the complete set of the acquired data for the different input voltages.

All the resistivity values obtained with different inputs are comparable [26], so with this particular geological condition there are no remarkable differences and benefits of using higher voltages. Same results are obtained with pole–dipole array. For this reason, the following analyses could be carried out using only one data set neglecting the influence of changing input voltages. Of course, it is not possible to generalize this statement based only on the analyzed data, since the results could be related to the local resistivity distribution and limited to the study area. Therefore, the data set used in the following analysis is that obtained employing an input voltage of 800 V.

To identify the electrode position, a Leica 1200 GPS was employed. The acceptable GPS error was set equal to 0.05 m, which means that if the uncertainty of GPS acquisition is lower than the threshold the measurement is directly accepted by the instrument, otherwise the operator evaluates if accept it or not. The instrument provides the value of the measurement and the error as $x = \widetilde{x} + \varepsilon$, where $\widetilde{x}$ is the position of the electrodes and $\varepsilon$ is the GPS error. Because of a nonfavorable satellite geometry (the mean DOP value was higher than 7 and the number of visible satellites was always lower than 6), a low quality of the transmission signal, and the presence of some olive trees, only the 11.0% of the data were stored with an error lower than 0.05 m, and among this only the 2.8% has an error lower than 0.03 m. Fig. 5 shows how the error $\varepsilon$ are distributed using a boxplot. The range of the acquired error is [0.0247 m, 0.9988 m], the median value is 0.4927 m and the mean is 0.4478 m. The above-mentioned nonfavorable conditions highly influence the data acquisition, leading to a very low quality of data.

The errors in Fig. 5 must be referred to the complete extension of the array, since the evaluation of the geometric factor is based on the distance between the electrodes and not on their absolute positions. The worst case (by uncertainty point of view) occurs when the shortest array is involved with the highest GPS error.

In the dipole–dipole array in the considered survey ($a = 1$, $n = 1$ and theoretical distance between electrodes of 1.5 m) the shortest array is 4.5 m long. Therefore, the maximum uncertainty value leads to an error of 22%. Considering a more realistic scenario with the same array but the mean value of uncertainty the error decreases to 10%. When far-distant electrodes are involved, the length of the array increases and consequently the percentage error decreases. For example, the largest array ($a = 5$, $n = 10$ and theoretical distance between electrodes of 1.5 m) is 90 m long. In case the maximum value of uncertainty is involved the percentage error is 1.1%, which decreases to 0.5% for the mean uncertainty value. For some types of applications (e.g., tomography applied in medical science) these high positioning error values are unacceptable, but in archeological and geophysics surveys could frequently occur. Since experimentally this aspect is neglected during the measurement campaign (as illustrated in the literature review in Section I), the idea of this article was to study a worst-case scenario to understand the influence of such high errors on the soil resistivity analysis.

Fig. 6 shows the real deployment of the 72 electrodes, represented by black dots. The figure highlights that the electrodes are not perfectly in line but some deviations, due to the imperfection of the soil and the human error in positioning, are present. All the values are related to the GPS acquisition.

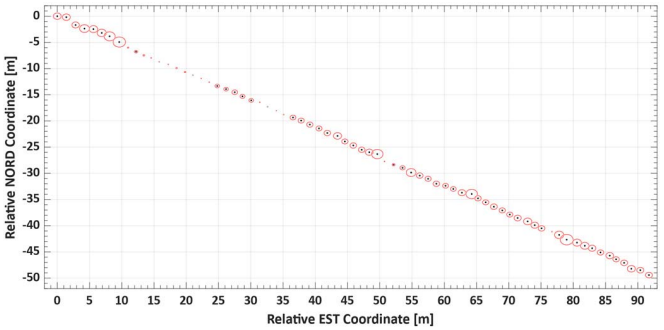


Fig. 6. Electrode position acquired using the GPS: the black dots represent the acquired values, and the red circles stand for the GPS errors of each electrode. The coordinates used are expressed in meters and are normalized with respect to the position of the first electrode.

The dots are surrounded by red circles, where the radius of each circle stands for the error $\varepsilon$ in the specific position. The used coordinate system is the projected Gauss-Boaga Roma40, normalized with respect to the position of the first electrode.

## IV. Proposed Approach

This section deals with MC simulation (MCS) to take into account the effects of the error in the positioning of the electrodes. MCS is based on multiple trial runs to approximate the outcomes of a certain event in terms of probability that the event occurs. It is a problem-solving method widely used in several different fields of application. The multiple runs are usually called simulations. Each simulation depends on a set of input variables randomly selected based on their probability density function. The model of the output is determined observing its statistical characteristics. The steps of the procedure illustrated in Fig. 7 are the following.

1) The input data must be acquired after the measurement survey (coordinates of the electrodes, sequence of acquisition, electrical parameters).
2) Construct a domain of electrode locations considering the ideal position of the electrodes and the error of the GPS measurement.
3) Set $i = 1$ and $N =$ number of MC simulations.
4) Generate the random position of the electrodes inside the domain according to the normal probability density function.
5) Following equations (4) and (5) the geometric factor $k$ and the apparent resistivity $\rho$ are calculated.
6) Steps 4 and 5 are reiterated up to $i = N$.
7) Statistical analysis of the final results.

Fig. 8 illustrates the domain of a generic position of the electrode A. The error in the location of the electrode (i.e., the data shown in Fig. 5) is used to calculate the standard deviation of the distribution, while the mean value is the ideal position.

Considering $\varepsilon$ the uncertainty of the GPS measurement related to the electrode A, the standard deviation of the distribution is evaluated considering the "empirical rule" as

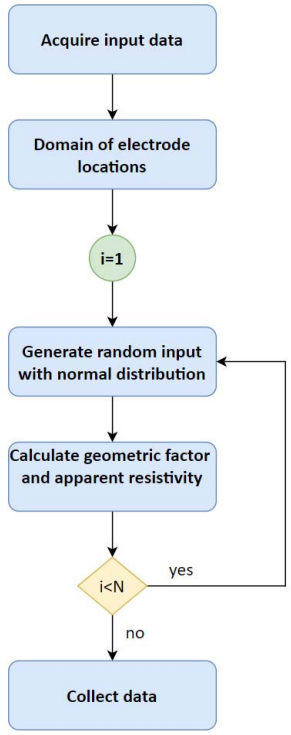


Fig. 7. Procedure used to generate multiple MC samples and analyze the effects of the error in the position of the electrodes.

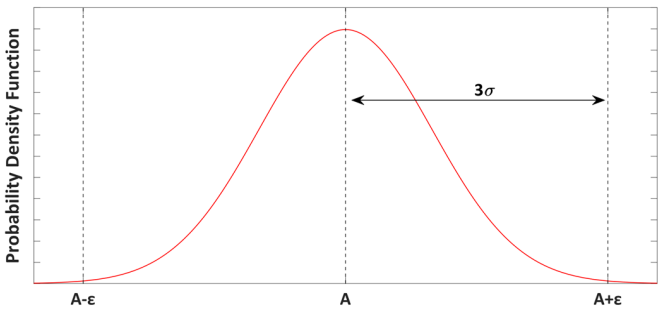


Fig. 8. Graphical representation of the Step 2 of the proposed MC procedure.

follows:

$$P(\mu - 3\sigma \leq X \leq \mu + 3\sigma) \approx 0.9973 \tag{16}$$

where X is the observation from the random variable, $\mu$ and $\sigma$ are the mean and the standard deviation of the distribution.

Therefore, the 99.73% of values lie within the range $[A - \varepsilon, A + \varepsilon]$ where the mean value $\mu$ was set equal to the position $A$. Consequently

$$3\sigma = \varepsilon \Rightarrow \sigma = \frac{\varepsilon}{3}. \tag{17}$$

This procedure for the domain construction is repeated for all the ideal positions of $A$, $B$, $M$, and $N$ electrodes; for each one of them, 100 000 samples are generated.

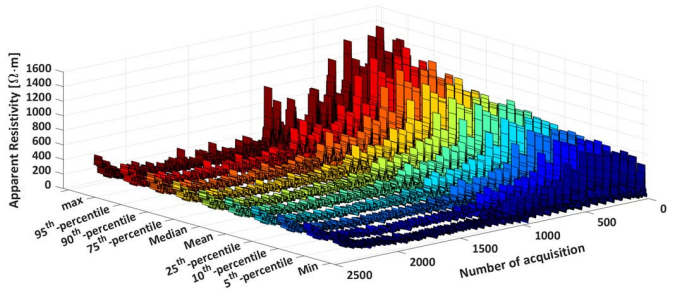


Fig. 9. Results of the MC simulation for the dipole–dipole array. Each color stands for a different statistical parameter. The 2475 different points of acquisition of each curve are ordered by increasing depth of investigation.

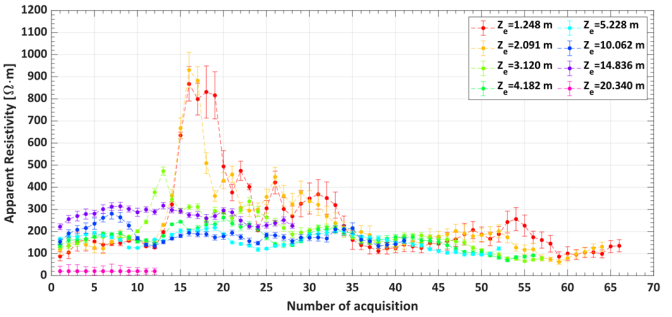


Fig. 10. Results of the MC simulation for some random depth of the dipole–dipole array, where each color stands for a different depth. Each point shows mean and standard deviation of the simulation.

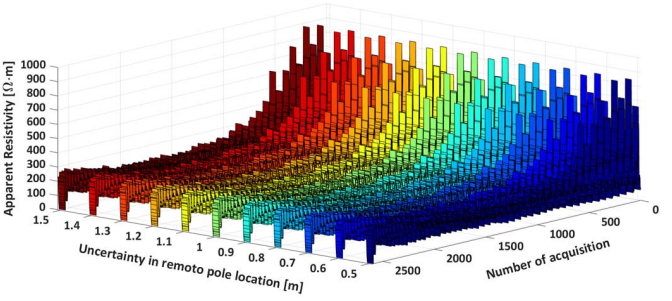


Fig. 11. Mean value of the MC simulation for the pole–dipole array varying the uncertainty in the positioning of the remote pole, where each color represents a different uncertainty value. The 2625 different points of acquisition of each curve are ordered by increasing depth of investigation.

## V. Results and Discussion

This section resumes the main results and striking observation of the MC simulation. The proposed approach has been applied to both P–D and D–D arrays, firstly considering the ideal in-line position of the electrodes affected by the error in Fig. 5 (this model will be called "Theoretical" in the following), then considering the real coordinates of the electrodes, i.e., considering the real topography of the measurement campaign including the errors illustrated in Fig. 6 (this model will be called "Real" in the following).

### *A. Results of Monte Carlo Simulations*

The MC simulation has proven to be a powerful method to evaluate the effects of the electrode positioning in the ERT measurement. Each D–D simulation provides a 2475 $\times$ 100000 samples, where 2475 are the number of different electrode acquisitions, and 100 000 are the number of MC repetitions, while the P–D simulations provide 2625 $\times$ 100 000 samples. Therefore, a statistical data analysis must be implemented to extrapolate the relevant information from the data set. Fig. 9 shows the apparent resistivity simulated for the dipole–dipole array in the "theoretical" configuration. The main statistical parameters are included in the chart using different colors. The samples are ordered by increasing the depth of investigation. The measured apparent resistivity varies in a range from 20 $\Omega$·m to 1200 $\Omega$·m where the highest values represent a possible underground anomaly and are all located in the first meters of investigation. By a statistic point of view, the mean value represents the optimal estimator for this kind of analysis. In spite of this, also other parameters must be considered since the differences between them are remarkable. The effects are more relevant for shallow depth, but they cannot be neglected also for deeper analysis. Same results were obtained also for the pole–dipole array. Therefore, all these statistical results are used to evaluate the true resistivity of the subsurface using the "inversion algorithm." In particular, the inversion algorithm is implemented after the MC simulation taking the apparent resistivity achieved using MCS as input to reconstruct the subsoil image. Consequently, it is really important to deeply analyze the results of the MC simulations since their outputs will have a significant impact on the true resistivity of the subsurface. The first findings achieved after the inversion procedure are illustrated in [36], while this section analyzes the effects of the error only on the apparent resistivity using the mean value of the data set for each acquisition.

Fig. 10 uses the error bar to illustrate the mean value and the standard deviation of some randomly chosen acquisitions of the dipole–dipole array ("Theoretical" simulation). Each trend identified with a unique color represents a different depth of investigation. As seen in Fig. 3, the deeper the analysis, the lower the number of acquisition points. The figure shows that for shallow depth the standard deviation is remarkable, while for deeper acquisition the error is smaller. Since for archeological purposes the depth of interested is generally limited to the first meters from the ground surface, this consideration must always be taken into account.

To overcome the problem, the following subsections compare different simulation results to identify the optimal array architecture for each different scenario.

### *B. Effects of Uncertainty in Remote Pole Positioning*

The right positioning of the remote pole is a challenging aspect on geophysical survey. It should be deployed as far as possible (theoretically infinite distance) from the array, but of course it is not possible due to finite length of the cable, geomorphological aspects, presence of obstacles, and so on. Moreover, when the optimal location is identified, trees or other obstacles could influence the quality of the GPS signal and the coordinate of the pole positioning could be affected by significant error. Therefore, this subsection analyzes the effects of the remote pole position on the measurement survey.

Fig. 11 shows the mean value of the MC simulation for the pole–dipole array varying the error $\varepsilon_{RP}$ in the positioning

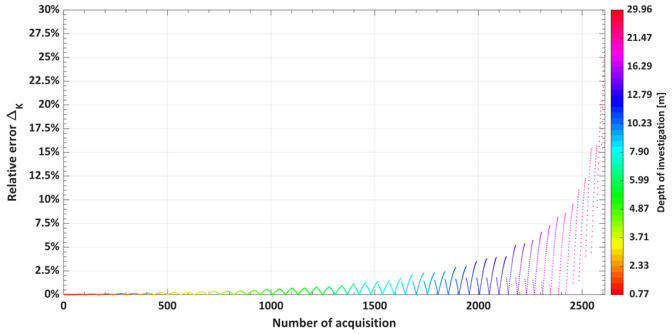


Fig. 12. Percentage relative error between geometric factors calculated considering infinite and real position of the remote pole. The error is ordered by increasing depth of investigation, and each depth is identified with a different color.

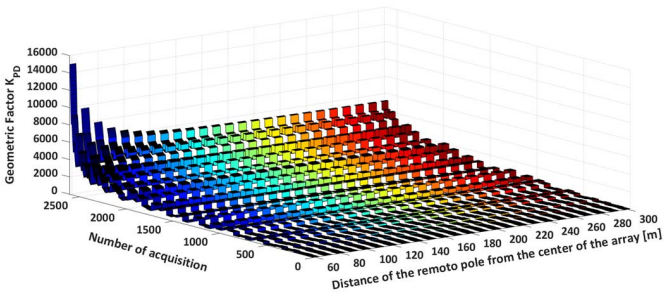


Fig. 13. Representation of all the 2625 values of the geometric factor for the pole–dipole array varying the $y$-coordinate of the remote pole, which means changing the distance of the electrode from the center of the array. Each color represents a different distance considered in the simulation.

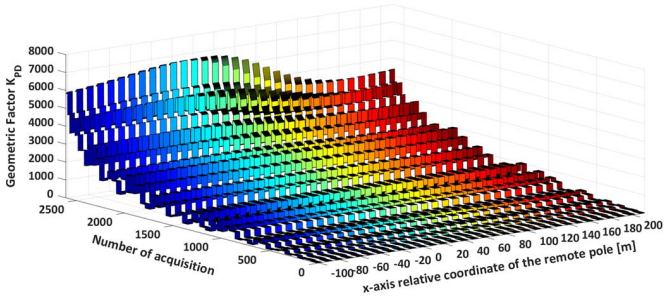


Fig. 14. Representation of all the 2625 values of the geometric factor for the pole–dipole array varying the $x$-coordinate of the remote pole, which means shifting the position of the electrode from one possible extreme of the array to another. Each color represents a different distance considered in the simulation.

of the remote pole. The different colors stand for different uncertainty values used in the simulation, from $\varepsilon_{\mathrm{RP}} = 0.5$ m to $\varepsilon_{\mathrm{RP}} = 1.5$ m.

The samples are ordered by increasing depth of investigation, from shallow to deeper acquisitions. The figure highlights that no significant differences are resulted in the different simulations. This is a remarkable result because a high GPS error in the acquisition of the remote pole location does not affect the measurement survey.

Since the uncertainty in the remote pole deployment does not influence the apparent resistivity, the effects of a noninfinite positioning were investigated considering the parameter $\Delta_K$ defined as the percentage relative error between the geometric factor considering the ideal infinite position of the remote pole $K_{\mathrm{PD}_\infty}$ and the actual geometric factor $K_{\mathrm{PD}}$ (calculated with the real coordinates of the remote pole)

$$\Delta_K = 100 \cdot \left| \frac{K_{\mathrm{PD}_\infty} - K_{\mathrm{PD}}}{K_{\mathrm{PD}_\infty}} \right|. \tag{18}$$

Using the coordinates of the remote pole (100 m perpendicularly far from the center of the array), Fig. 12 shows the influence of a noninfinite positioning of the remote pole at different depths and for different electrode acquisitions.

Particularly, the analyzed error increases when the depth of investigation increases, showing a significant influence of the remote pole positioning when the investigation depth is greater than 15 m (with a corresponding maximum value of the error of approximately 5%).

The most striking result to emerge from the simulation is that: fixing the depth of investigation, the data describe a sort of "v trend," with an initial decreasing phase followed by an ascending phase. The error is minimized when the dipole of acquisition is perpendicular to the remote pole.

Despite this behavior, for archeological purpose the depth of investigation is shallow, and generally it is lower than 15 m. In this scenario, the relative error is low, highlighting that the real positioning of the remote pole has no significant effects on the measurement survey.

Geophysical literature demonstrates that the optimal positioning of the remote pole is perpendicular to the center of the array, with a distance at least equal to the total length of the array (106.5 m in the analyzed survey). Since it is not always neither easy nor possible to ensure this scenario, the following analyses simulate the geometric factor of the pole–dipole array varying $y$- and $x$-coordinates of the remote pole.

Fig. 13 shows the effects of the moving of the remote pole from the center of the array (in other words the simulation shows the geometric factor increasing the $y$-coordinate of the electrode). In the figure, $K_{\mathrm{PD}}$ is ordered by increasing depth of investigation.

The figure highlights that the variation of the geometric factor increases as the distance tends to decrease, producing a stabilization of the geometric factor.

For distance higher than 130 m the variation of the geometric factor is negligible, while for distance lower than 100 m the obtained geometric factor is not trustworthy and consequently the measured resistivity will not be reliable. This effect is more evident for deeper analysis, while for shallow investigation lower distance of the remote pole is acceptable.

Fig. 14 shows the effects of the moving of the remote pole on the $x$-axis, fixing the $y$-coordinate to 100 m. The range of the simulation varies from $-100$ to 200 m, the subrange between 0 and 100 m is the actual position of the other electrodes. If the remote pole is located on the left of the array, the geometric factor is higher than $K_{\mathrm{PD}_\infty}$, while whether the remote pole is located on the right side of the array, the geometric factor is lower than $K_{\mathrm{PD}_\infty}$.

In summary, these analyses highlight that the remote pole should be located perpendicularly from the center of the array to minimize the effect of a noninfinite positioning on the $x$-axis. The minimum acceptable distance from the center of the array is equal to the length of the array itself. The

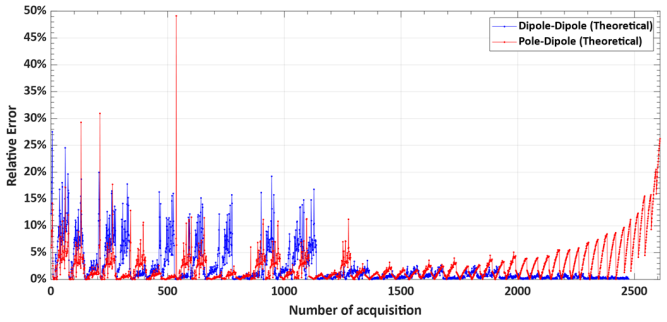


Fig. 15. Percentage relative error between the apparent resistivity measurements and the mean value of the apparent resistivity simulated using MC approach considering the dipole–dipole array (blue line) and the pole–dipole array (red line). Both trends refer to the in-line electrode analysis ("Theoretical" configuration).

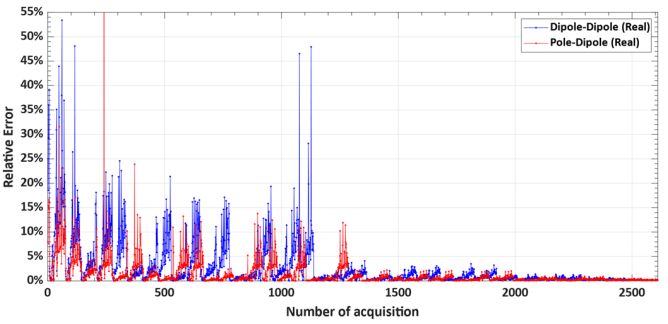


Fig. 16. Percentage relative error between the apparent resistivity measurements and the mean value of the apparent resistivity simulated using MC approach considering the dipole–dipole array (blue line) and the pole–dipole array (red line). In both trends the real topography of the measurement survey is considered.

higher the distance, the lower the effects of the noninfinite positioning, especially for shallow depths.

Nevertheless, it is not necessary to reach further location since the difference in the geometric factor is negligible. A distance equal to the length of the array represents the optimal trade-off between the minimization of the error and the possible installation.

### *C. Comparison Between Pole–Dipole and Dipole–Dipole Arrays*

In this subsection, the results of the simulation for the pole–dipole array and dipole–dipole array are compared to investigate which is the best one for archeological purpose. The first results illustrated in Fig. 15 refer to the "theoretical" scenario in which the real topography of the survey is neglected, and the electrodes are supposed to be in-line. The blue line stands for the percentage relative error $\mathrm{RE}_{\mathrm{DD-Th}}$ between the measurement acquisition $\rho_{\mathrm{DD\_mea}}$ and the mean value of the simulation $\widetilde{\rho^{\mathrm{Th}}_{\mathrm{DD\_sim}}}$ of the D–D array, while the red trend represents the percentage relative error $\mathrm{RE}_{\mathrm{PD-Th}}$ between the measurement acquisition $\rho_{\mathrm{PD\_mea}}$ and the mean value of the simulation $\widetilde{\rho^{\mathrm{Th}}_{\mathrm{PD\_sim}}}$ of the P–D array. Both errors are evaluated using the following equations:

$$\mathrm{RE}_{\mathrm{DD-Th}} = 100 \cdot \left| \frac{\rho_{\mathrm{DD\_mea}} - \widetilde{\rho^{\mathrm{Th}}_{\mathrm{DD\_sim}}}}{\rho_{\mathrm{DD\_mea}}} \right| \tag{19}$$

$$\mathrm{RE}_{\mathrm{PD-Th}} = 100 \cdot \left| \frac{\rho_{\mathrm{PD\_mea}} - \widetilde{\rho^{\mathrm{Th}}_{\mathrm{PD\_sim}}}}{\rho_{\mathrm{PD\_mea}}} \right|. \tag{20}$$

The errors in Fig. 15 are ordered by increasing the depth of investigation, highlighting that the effects of the error in the electrode positioning are relevant for both arrays at shallow depth. The high values of the relative error are mainly due to the fact that the errors in the electrode positioning were very remarkable due to nonfavorable conditions during the survey. Nevertheless, the P–D array shows a relative error lower than the P–D array on average at shallow depth. Quite the opposite, for depth greater than 10 m, $\mathrm{RE}_{\mathrm{DD-FLAT}}$ decreases tending to negligible values, while $\mathrm{RE}_{\mathrm{PD-FLAT}}$ increases maintaining the "v shape" highlighted also in Fig. 12.

Fig. 16 shows the results of the simulation introducing the real topography of the survey.

In this scenario, the electrodes are not in-line, but the coordinate, the altitude, and the GPS error are considered (see Fig. 6). The blue line stands for the percentage relative error $\mathrm{RE}_{\mathrm{DD-Real}}$ between the measurement acquisition $\rho_{\mathrm{DD\_mea}}$ and the mean value of the simulation $\widetilde{\rho^{\mathrm{Real}}_{\mathrm{DD\_sim}}}$ of the D–D array, while the red trend represents the percentage relative error $\mathrm{RE}_{\mathrm{PD-Real}}$ between the measurement acquisition $\rho_{\mathrm{PD\_mea}}$ and the mean value of the simulation $\widetilde{\rho^{\mathrm{Real}}_{\mathrm{PD\_sim}}}$ of the P–D array. The errors are evaluated as follows:

$$\mathrm{RE}_{\mathrm{DD-Real}} = 100 \cdot \left| \frac{\rho_{\mathrm{DD\_mea}} - \widetilde{\rho^{\mathrm{Real}}_{\mathrm{DD\_sim}}}}{\rho_{\mathrm{DD\_mea}}} \right| \tag{21}$$

$$\mathrm{RE}_{\mathrm{PD-Real}} = 100 \cdot \left| \frac{\rho_{\mathrm{PD\_mea}} - \widetilde{\rho^{\mathrm{Real}}_{\mathrm{PD\_sim}}}}{\rho_{\mathrm{PD\_mea}}} \right|. \tag{22}$$

Also in this case, the analyzed errors are ordered by increasing depth of investigation. In these simulations, the analyzed relative errors have comparable trends with the "theoretical simulation," on average. At shallow depth, the D–D array seems to be more affected by the GPS error with respect to the P–D array, while for greater depth the influence of the error is negligible.

These analyses are useful to decide which type of array is the most suitable depending on the scenario that will be investigated. For instance, for archeological investigation of tumuli, the P–D array has a lower influence of the GPS error with respect to the D–D array in the depth of interest. Quite the opposite, in case of deeper investigation, the dipole–dipole array is the most suitable solution.

### *D. Pros and Cons in the Introduction of the* Real *Topography*

The final simulations taken into account consider the real topography of the survey to evaluate if there are remarkable advantages in the use of the topography instead of the in-line simulation. Moreover, also the GPS error in both EST and NORD coordinates is considered. The blue line in Fig. 17 represents the relative error $\mathrm{RE}_{\mathrm{PD-FLAT}}$, while the red trend stands for the percentage relative error $\mathrm{RE}_{\mathrm{PD-TOPO}}$.

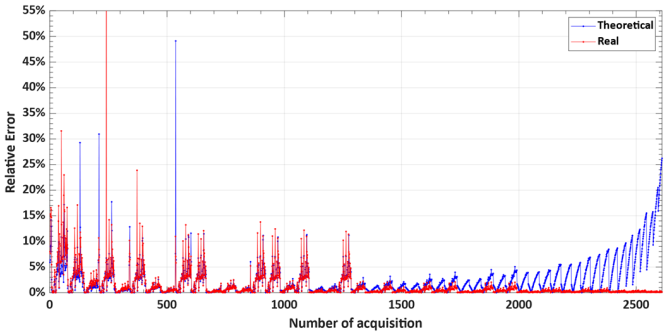


Fig. 17. Percentage relative error between the apparent resistivity measurements and the mean value of the apparent resistivity simulated using MC approach considering the "Theoretical" scenario (blue line) and the "Real" simulation (red line). Both trends refer to the pole–dipole array.

Fig. 17 highlights that the "real" simulation allows to reduce the influence of the GPS error at all the investigated depths.

This advantage is relevant especially at high depth, in which in the in-line simulation the error increase, while introducing the topography ("Real" simulation) the error is quite stable.

The advantages of the topography are also investigated in case of dipole–dipole array introducing a new parameter, the percentage relative error $\mathrm{RE_{DD}}$ between the mean value of the simulation considering the real topography $\widetilde{\rho^{\mathrm{Real}}_{\mathrm{DD\_sim}}}$ and the mean value of the simulation in the in-line scenario $\widetilde{\rho^{\mathrm{Th}}_{\mathrm{DD\_sim}}}$, evaluated as follows:

$$\mathrm{RE_{DD}} = 100 \cdot \left| \frac{\widetilde{\rho^{\mathrm{Real}}_{\mathrm{DD\_sim}}} - \widetilde{\rho^{\mathrm{Th}}_{\mathrm{DD\_sim}}}}{\widetilde{\rho^{\mathrm{Real}}_{\mathrm{DD\_sim}}}} \right|. \tag{23}$$

Fig. 18 illustrates $\mathrm{RE_{DD}}$ ordered by increasing depth of investigation, where each color represents a different depth. The error between considering or not the topography is remarkable regardless of the depth of investigation. Increasing the depth, the influence of the topography slightly decreases but still remains a considerable effect. This means that, the introduction of the real topography inside the procedure is mandatory because it influences the measurement even more than the GPS error.

## VI. Conclusion

The aim of this study was to investigate the effects of the GPS error in the location of the electrodes for ERT on resistivity measurement. An ERT survey was carried out on Poggio Pepe tumulus near Vetulonia (Italy), with the aim to verify the presence of an Etruscan tomb and optimize the archeological excavation. Seventy-two electrodes plus a remote pole were used to implement both dipole–dipole and pole–dipole arrays.

An MC simulation is taken into account in this article to evaluate how the GPS errors in the electrode deployment influence the survey.

The proposed approach has been applied to four different scenarios: P–D array with in-line electrodes, D–D array with in-line electrodes, P–D array introducing the effects of the real topography, and D–D array considering the effect of topography.

One of the more significant findings to emerge from this study is related to the positioning of the remote pole in

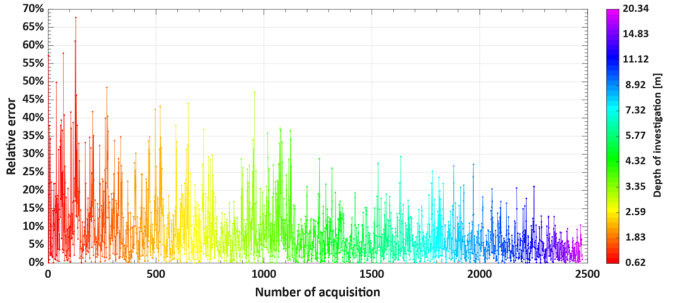


Fig. 18. Percentage relative error between mean value of the apparent resistivity simulated using MC approach considering the "Theoretical" scenario and the "Real" simulation. Both trends refer to the dipole–dipole array.

the P–D array. Simulations have been repeated considering the influence of the uncertainty in the remote pole location and considering variations on the pole coordinates. These findings have significant implications for the understanding of where the remote pole should be located. In particular, in contrast to all the other electrodes in the array, the uncertainty of the remote pole positioning does not affect the resistivity measurement, while a proper distance from the array is mandatory. To minimize the effects of a noninfinite positioning, the remote pole should be located perpendicularly to the center of the ERT line, at a distance at least equal to the length of the array itself. Moreover, the study suggests that it is not necessary to reach further location since the geometric factor remains almost the same.

Finally, the four different scenarios are compared to identify when and how to use an array or the other, and when the topography must use rather than the in-line situation. What stands from the simulations is that the pole–dipole array suffers lower influence of the GPS error at shallow depths, proving that it is a more suitable method for archeological purposes. Quite the opposite, for deeper investigation the dipole–dipole is preferable. Moreover, the topography of the survey must always be considered during the inversion procedure because it influences the measurement even more than the GPS error.

In conclusion, the simulations carried out for this project refer to a very extreme acquisition of the error, and consequently could be considered as worst case. Therefore, also the error on the apparent resistivity is remarkable. If the error on the resistivity measurement that comes out from the simulation is not acceptable, then in case of nonfavorable conditions for the GPS, the measurement campaign should be rescheduled another day. A high quality of the measurement data set will lead to an optimization of the localization of the archeological target, with a minimization of the costs.

## Acknowledgment

The authors would like to thank Angelo (the owner of the field where Poggio Pepe Tumulos is located) and the "Soprintendenza Archeologia Belle Arti e Paesaggio for the Provinces of Arezzo, Siena and Grosseto" to let them carry out the measurements.

## References

[1] L. Busato *et al.*, "Combined geophysical surveys for the characterization of a reconstructed river embankment," *Eng. Geol.*, vol. 211, pp. 74–84, Aug. 2016.

[2] C. Jodry, S. Palma Lopes, Y. Fargier, P. Côte, and M. Sanchez, "A cost-effective 3D electrical resistivity imaging approach applied to dike investigation," *Near Surf. Geophysics*, vol. 15, no. 1, pp. 27–41, Feb. 2017.

[3] M. H. Loke, J. E. Chambers, D. F. Rucker, O. Kuras, and P. B. Wilkinson, "Recent developments in the direct-current geoelectrical imaging method," *J. Appl. Geophys.*, vol. 95, pp. 135–156, Aug. 2013.

[4] V. Pazzi, M. Ceccatelli, T. Gracchi, E. B. Masi, and R. Fanti, "Assessing subsoil void hazards along a road system using H/V measurements, ERTs and IPTs to support local decision makers," *Near Surf. Geophys.*, vol. 16, no. 3, pp. 282–297, Jun. 2018.

[5] V. Pazzi *et al.*, "Integrated geophysical survey in a sinkhole-prone area: Microgravity, electrical resistivity tomographies, and seismic noise measurements to delimit its extension," *Eng. Geol.*, vol. 243, pp. 282–293, Sep. 2018.

[6] V. Pazzi, S. Morelli, and R. Fanti, "A review of the advantages and limitations of geophysical investigations in landslide studies," *Int. J. Geophys.*, vol. 2019, Jul. 2019, Art. no. 2983087.

[7] F. A. M. Santos and A. R. A. Afonso, "Detection and 2D modelling of cavities using pole–dipole array," *Environ. Geol.*, vol. 48, no. 1, pp. 108–116, Jun. 2005.

[8] S. Uhlemann *et al.*, "Interpolation of landslide movements to improve the accuracy of 4D geoelectrical monitoring," *J. Appl. Geophys.*, vol. 121, pp. 93–105, Oct. 2015.

[9] A. Binley, G. Cassiani, and R. Deiana, "Hydrogeophysics—Opportunities and challenges," *Boll. di Geofis. Teor. ed Appl.*, vol. 51, no. 4, pp. 267–284, 2010.

[10] A. Binley *et al.*, "The emergence of hydrogeophysics for improved understanding of subsurface processes over multiple scales," *Water Resour. Res.*, vol. 51, no. 6, pp. 3837–3866, Jun. 2015.

[11] G. M. Maillet, E. Rizzo, A. Revil, and C. Vella, "High resolution electrical resistivity tomography (ERT) in a transition zone environment: Application for detailed internal architecture and infilling processes study of a Rhône River Paleo-channel," *Mar. Geophys. Res.*, vol. 26, nos. 2–4, pp. 317–328, Jun. 2005.

[12] F. Fischanger, G. Morelli, G. Ranieri, G. Santarato, and M. Occhi, "4D cross-borehole electrical resistivity tomography to control resin injection for ground stabilization: A case history in Venice (Italy)," *Near Surf. Geophys.*, vol. 11, no. 1, pp. 41–50, Feb. 2013.

[13] G. Santarato, G. Ranieri, M. Occhi, G. Morelli, F. Fischanger, and D. Gualerzi, "Three-dimensional electrical resistivity tomography to control the injection of expanding resins for the treatment and stabilization of foundation soils," *Eng. Geol.*, vol. 119, nos. 1–2, pp. 18–30, Apr. 2011.

[14] R. Clement and S. Moreau, "How should an electrical resistivity tomography laboratory test cell be designed? Numerical investigation of error on electrical resistivity measurement," *J. Appl. Geophys.*, vol. 127, pp. 45–55, Apr. 2016.

[15] P. B. Wilkinson, J. E. Chambers, M. Lelliott, G. P. Wealthall, and R. D. Ogilvy, "Extreme sensitivity of crosshole electrical resistivity tomography measurements to geometric errors," *Geophys. J. Int.*, vol. 173, no. 1, pp. 49–62, Apr. 2008.

[16] V. Pazzi, D. Tapete, L. Cappuccini, and R. Fanti, "An electric and electromagnetic geophysical approach for subsurface investigation of anthropogenic mounds in an urban environment," *Geomorphology*, vol. 273, pp. 335–347, Nov. 2016.

[17] A. Tejero-Andrade, D. L. Argote-Espino, G. Cifuentes-Nava, E. Hernández-Quintero, R. E. Chávez, and A. García-Serrano, "'Illuminating' the interior of Kukulkan's pyramid, Chichén Itzá, mexico, by means of a non-conventional ERT geophysical survey," *J. Archaeol. Sci.*, vol. 90, pp. 1–11, Feb. 2018.

[18] G. N. Tsokas *et al.*, "ERT imaging of the interior of the huge Tumulus of Kastas in Amphipolis (Northern Greece)," *Archaeol. Prospection*, vol. 25, no. 4, pp. 347–361, Oct. 2018.

[19] P. Tsourlos, N. Papadopoulos, M.-J. Yi, J.-H. Kim, and G. Tsokas, "Comparison of measuring strategies for the 3-D electrical resistivity imaging of tumuli," *J. Appl. Geophys.*, vol. 101, pp. 77–85, Feb. 2014.

[20] A. Arato, S. Piro, and L. Sambuelli, "3D inversion of ERT data on an archaeological site using GPR reflection and 3D inverted magnetic data as *a priori* information," *Near Surf. Geophys.*, vol. 13, no. 6, pp. 545–556, Dec. 2015.

[21] N. G. Papadopoulos, P. Tsourlos, G. N. Tsokas, and A. Sarris, "Efficient ERT measuring and inversion strategies for 3D imaging of buried antiquities," *Near Surf. Geophys.*, vol. 5, no. 6, pp. 349–361, Dec. 2007.

[22] N. G. Papadopoulos, M.-J. Yi, J.-H. Kim, P. Tsourlos, and G. N. Tsokas, "Geophysical investigation of tumuli by means of surface 3D electrical resistivity tomography," *J. Appl. Geophys.*, vol. 70, no. 3, pp. 192–205, Mar. 2010.

[23] G. A. Oldenborger, P. S. Routh, and M. D. Knoll, "Sensitivity of electrical resistivity tomography data to electrode position errors," *Geophys. J. Int.*, vol. 163, no. 1, pp. 1–9, Oct. 2005.

[24] S. Szalai, A. Koppán, and L. Szarka, "Effect of positional inaccuracies on multielectrode results," *Acta Geodaetica et Geophysica Hungarica*, vol. 43, no. 1, pp. 33–42, Mar. 2008.

[25] B. Zhou and T. Dahlin, "Properties and effects of measurement errors on 2D resistivity imaging surveying," *Near Surf. Geophys.*, vol. 1, no. 3, pp. 105–117, Aug. 2003.

[26] A. D. Parsekian *et al.*, "Comparing measurement response and inverted results of electrical resistivity tomography instruments," *J. Environ. Eng. Geophys.*, vol. 22, no. 3, pp. 249–266, Sep. 2017.

[27] A. P. Aizebeokhai and A. I. Olayinka, "Anomaly effects of orthogonal paired-arrays for 3D geoelectrical resistivity imaging," *Environ. Earth Sci.*, vol. 64, no. 8, pp. 2141–2149, Dec. 2011.

[28] T. Dahlin and B. Zhou, "A numerical comparison of 2D resistivity imaging with 10 electrode arrays," *Geophys. Prospecting*, vol. 52, no. 5, pp. 379–398, Sep. 2004.

[29] T. Hennig, A. Weller, and T. Canh, "The effect of dike geometry on different resistivity configurations," *J. Appl. Geophys.*, vol. 57, no. 4, pp. 278–292, Jul. 2005.

[30] W. Al-fares and M. Al-hilal, "Integration of electrical resistivity tomography with electromagnetic and soil radon measurements for characterizing the leakage problem in Afamia B dam, Syria," *Geofísica Internacional*, vol. 57, no. 4, pp. 275–287, 2018.

[31] M. Fressard, O. Maquaire, Y. Thiery, R. Davidson, and C. Lissak, "Multi-method characterisation of an active landslide: Case study in the Pays d'Auge plateau (Normandy, France)," *Geomorphology*, vol. 270, pp. 22–39, Oct. 2016.

[32] A. Viero, A. Galgaro, G. Morelli, A. Breda, and R. G. Francese, "Investigations on the structural setting of a landslide-prone slope by means of three-dimensional electrical resistivity tomography," *Natural Hazards*, vol. 78, no. 2, pp. 1369–1385, Sep. 2015.

[33] M. Karaim, M. Elsheikh, and A. Noureldin, "GNSS error sources," in *Multifunctional Operation and Application of GPS*. Rijeka, Croatia: InTech, 2018.

[34] J. Van Sickle, *GPS for Land Surveyors*, 4th ed. Boca Raton, FL, USA: CRC Press, 2015.

[35] V. Pazzi *et al.*, "ERT investigation of tumuli: Does the errors in locating electrodes influence the resistivity?" in *Proc. IMEKO TC-4 Int. Conf. Metrol. Archaeol. Cultural Heritage*, 2019, pp. 527–532.

[36] V. Pazzi *et al.*, "Analysis of the influence of the GPS errors occurred while collecting electrode coordinates on the electrical resistivity of tumuli," *Sensors*, vol. 20, no. 10, p. 2966, May 2020.

[37] C. Matthews, P. Clarkson, P. M. Harris, W. G. Kurten Ihlenfeld, and P. S. Wright, "Evaluation of flicker measurement uncertainties by a Monte Carlo method," *IEEE Trans. Instrum. Meas.*, vol. 60, no. 7, pp. 2255–2261, Jul. 2011.

[38] S. S. Agili, A. W. Morales, J. Li, and M. Resso, "Finding the probability distribution functions of S-parameters and their Monte Carlo simulation," *IEEE Trans. Instrum. Meas.*, vol. 61, no. 11, pp. 2993–3002, Nov. 2012.

[39] N. Locci, C. Muscas, and S. Sulis, "Modeling ADC nonlinearity in Monte Carlo procedures for uncertainty estimation," *IEEE Trans. Instrum. Meas.*, vol. 55, no. 5, pp. 1671–1676, Oct. 2006.

[40] H. Germer, "High-precision AC measurements using the Monte Carlo method," *IEEE Trans. Instrum. Meas.*, vol. 50, no. 2, pp. 457–460, Apr. 2001.

[41] A. Ferrero and S. Salicone, "A comparison between the probabilistic and possibilistic approaches: The importance of a correct metrological information," *IEEE Trans. Instrum. Meas.*, vol. 67, no. 3, pp. 607–620, Mar. 2018.

[42] T. Dahlin, "2D resistivity surveying for environmental and engineering applications," *1st Break*, vol. 14, no. 7, pp. 275–283, Jul. 1996.

[43] S. Milun, T. Kilic, and O. Bego, "Measurement of soil thermal properties by spherical probe," *IEEE Trans. Instrum. Meas.*, vol. 54, no. 3, pp. 1219–1226, Jun. 2005.

[44] J. S. Sumner, *Principles of Induced Polarization for Geophysical Exploration*, 1st ed. Amsterdam, The Netherlands: Elsevier, 1976.

[45] D. D. Werkema, E. Atekwana, W. Sauck, and J. A. Asumadu, "A generic automated/semiautomated digital multi-electrode instrument for field resistivity measurements," *IEEE Trans. Instrum. Meas.*, vol. 49, no. 6, pp. 1249–1253, Jun. 2000.

[46] L. S. Edwards, "A modified pseudosection for resistivity and IP," *Geophysics*, vol. 42, no. 5, pp. 1020–1036, Aug. 1977.

**Lorenzo Ciani** (Senior Member, IEEE) received the M.S. degree in electronic engineering and the Ph.D. degree in industrial and reliability engineering from the University of Florence, Florence, Italy, in 2005 and 2009, respectively.

He is currently an Assistant Professor with the Department of Information Engineering, University of Florence. He has authored or coauthored more than 120 peer-reviewed journal articles and conference papers. His current research interests include system reliability, availability, maintainability and safety, reliability evaluation test and analysis for electronic systems and devices, fault detection and diagnosis, and electrical and electronic instrumentation and measurement.

Dr. Ciani is a member of the IEEE IMS TC-32 Fault Tolerant Measurement Systems and an Associate Editor of IEEE ACCESS and the IEEE TRANSACTION ON INSTRUMENTATION AND MEASUREMENT. He received the 2015 IEEE I&M Outstanding Young Engineer Award for his contribution to the advancement of instrumentation and measurement in the fields of reliability analysis.

**Marcantonio Catelani** (Member, IEEE) received the M.S. degree in electronic engineering from the University of Florence, Florence, Italy, in 1984.

He is currently with the Department of Information Engineering, University of Florence. Strictly correlated with reliability, availability, maintainability and safety (RAMS) are the fields of interest of both the fault diagnosis and reliability testing for components and equipment. In particular, the research activity concerns the development of test profiles used both for the characterization and the evaluation of reliability performance and, at the same time, the development of new degradation models able to estimate the life cycle of electronic components. His current research interests include development of automatic measurement system, the characterization of A/D converters, quality control and related statistical methods, and RAMS context.

**Giulia Guidi** (Student Member, IEEE) received the B.S. degree in electronic and telecommunications engineering and the M.S. degree in electronics engineering from the University of Florence, Florence, Italy, in 2015 and 2018, respectively, where she is currently pursuing the Ph.D. degree in industrial and reliability engineering.

Her research activities are concentrates in the fields of reliability analysis, optimization of availability and maintainability for railway application.

**Gabriele Patrizi** (Student Member, IEEE) received the B.S. degree in electronic and telecommunications engineering and the M.S. degree in electronics engineering from the University of Florence, Florence, Italy, in 2015 and 2018, respectively, where he is currently pursuing the Ph.D. degree in industrial and reliability engineering.

His research activities are concentrates in the fields of reliability, availability, maintainability and safety (RAMS) models and experimental analysis for complex systems used in industrial applications.

**Luca Cappuccini** is currently a Professor of etruscology with the Department of History, Archeology, Geography, Fine and Performing Arts, University of Florence, Florence, Italy. He is also the Scientific Director of the University Archeological Excavations, Monte Giovi (ager faesulanus, Florence, Italy) and San Germano (ager vetuloniensis, Grosseto, Italy). He is also a Scientific Collaborator of the University of Zurich, Zurich, Switzerland, on the archeological mission and research on the Etruscan culture. He has authored or coauthored more than 70 peer-reviewed journal articles and conference papers.

**Nicola Casagli** received the degree in geological science, the M.Sc. degree in engineering rock mechanics, and the Ph.D. degree in engineering geology from the Imperial College of London, London, U.K., 1989, 1992, and 1994, respectively.

He was an Expert of geological hazards and ground instability, monitoring technology, remote sensing, engineering geological characterization and modeling. He was the President of the National Institute of Oceanography and Applied Geophysics and the Civil Protection Center of University of Florence. He was a Founder and President-Elect of the International Consortium on Landslides (ICL). He was a member of the Major Risks National Committee of the Department of Civil Protection of the Italian Government and the World Center of Excellence on Landslide Risk Reduction of the International Program on Landslides. He was a Founder and an Associate of the UNESCO Chair on Prevention and Sustainable Mitigation of Geohydrological Hazards. He was an Adjunct Professor of the UNESCO Chair on Geoenvironmental Disaster Reduction at Shimane University (Japan). He was a member and former Vice President of the International Consortium on Geo-disaster Reduction (ICGdR). He was the Head of the Department of Earth Sciences and Past Member of the Academic Senate of the University of Florence. He is currently a Professor of engineering geology with the Earth Sciences Department, University of Florence. He was a Florence Ambassador. He is the author of more than 500 scientific publications. He holds four industrial patents.

Dr. Casagli was Awarded with the Order of Merit of the Italian Republic (4th Class Officer).

**Mattia Ceccatelli** was born in Florence, Italy, in 1991. He received the B.S. degree in earth sciences and the M.S. degree in earth sciences and technologies from the University of Florence, Florence, in 2013 and 2015, respectively, where he is currently pursuing the Ph.D. degree in civil and environmental engineering.

In 2019, he joined the Hydraulic Engineering Institute, Technische Universitat Braunschweig, Braunschweig, Germany, as a Visiting Researcher, where he was involved in the hydrologic and hydrogeologic modeling field. He is currently a Researcher with the Engineering Geology Group, Earth Sciences Department, University of Florence.

**Veronica Pazzi** received the M.Sc. degree in environmental engineering (with a thesis on geophysical methods applied to geo-archeological problems) and the Ph.D. degree in civil and environmental engineering (with a thesis on geophysical methods applied to environmental problems) from the University of Firenze, Florence, Italy, in 2007 and 2011, respectively.

Since 2011, she has been a Post-Doctoral Researcher with the Department of Earth Sciences, University of Firenze, where she also collaborates with the Center for the Civil Protection. Her research interests mainly include geophysical investigations, especially electrical resistivity and passive seismic methods, applied to slope instability and archeological problems. Moreover, her field of application is the development of methods for hazard, vulnerability, risk, and resilience assessment with also a special attention to buildings (especially schools) and cultural heritage sites.

Dr. Pazzi is a member of SEG, EAGE, EGU, IAEG Italian Section, and AIGA societies.